

# 1 Reconstruction of a daily gridded snow water equivalent product for 2 the land region above 45° N based on a ridge regression machine 3 learning approach

4 Donghang Shao<sup>1,2</sup>, Hongyi Li<sup>1,2</sup>, Jian Wang<sup>1,2</sup>, Xiaohua Hao<sup>1,2</sup>, Tao Che<sup>1,2</sup> and Wenzheng Ji<sup>1,2</sup>

5 <sup>1</sup>Northwest Institute of Eco-Environment and Resources, Chinese Academy of Sciences, Lanzhou, 730000, China

6 <sup>2</sup>Heihe Remote Sensing Experimental Research Station, Key Laboratory of Remote Sensing of Gansu Province, Chinese  
7 Academy of Sciences, Lanzhou, 730000, China

8 *Correspondence to:* Hongyi Li (lihongyi@lzb.ac.cn)

9 **Abstract.** The snow water equivalent (SWE) is an important parameter of the surface hydrological and climate systems, and  
10 it has a profound impact on Arctic amplification and climate change. However, there are great differences among existing  
11 SWE products. In the land region above 45° N, the existing SWE products are associated with a limited time span and  
12 limited spatial coverage, and the spatial resolution is coarse, which greatly limits the application of SWE data in cryosphere  
13 change and climate change studies. In this study, utilizing the ridge regression model (RRM) of a machine learning  
14 algorithm, we integrated various existing SWE products to generate a spatiotemporally seamless and high-precision RRM  
15 SWE product. The results show that it is feasible to utilize a ridge regression model based on a machine learning algorithm  
16 to prepare SWE products on a global scale. We evaluated the accuracy of the RRM SWE product using hemispheric-scale  
17 snow course (HSSC) observational data and Russian snow survey data. The MAE, RMSE, R, and R<sup>2</sup> between the RRM  
18 SWE products and observed SWEs are 0.21, 25.37 mm, 0.89, and 0.79, respectively. The accuracy of the RRM SWE dataset  
19 is improved by 28%, 22%, 37%, 11%, and 11% compared with the original AMSR-E/AMSR2 (SWE), ERA-Interim SWE,  
20 Global Land Data Assimilation System (GLDAS) SWE, GlobSnow SWE, and ERA5-land SWE datasets, respectively, and it  
21 has a higher spatial resolution. The RRM SWE product production method does not rely too much on an independent SWE  
22 product, it makes full use of the advantages of each SWE dataset, and it considers the altitude factor. The average MAE and  
23 RMSE of the RRM SWE products are 0.22 and 19.92 mm at different altitude intervals and 0.21 and 27.00 mm at different  
24 regions, respectively. This method has good stability, it is extremely suitable for the production of snow datasets with large

25 spatial scales, and it can be easily extended to the preparation of other snow datasets. The RRM SWE product is expected to  
26 provide more accurate SWE data for the hydrological model and climate model and provide data support for cryosphere  
27 change and climate change studies. The RRM SWE product is available from the ‘A Big Earth Data Platform for Three  
28 Poles’ (<http://dx.doi.org/10.11888/Snow.tpd.271556>) (Li et al., 2021).

## 29 **1 Introduction**

30 The IPCC (Intergovernmental Panel on Climate Change) AR6 (Sixth Assessment Report) notes that the Northern  
31 Hemisphere spring snow cover has greatly decreased since 1950, and the feedback effect of the climate system caused by  
32 this reduction is extremely large (Masson-Delmotte et al., 2021). In most land areas of the Northern Hemisphere, annual  
33 runoff is dominated by snowmelt, and accurately estimating the impacts of such a large amount of snowmelt runoff on  
34 ecosystems and human activities is of great significance (Barnett et al., 2005; Bintanja and Andry, 2017; Henderson et al.,  
35 2018). Whether through hydrometeorological simulation or global change research, the estimation of energy budget and  
36 mass of snow is very difficult, so a set of highly accurate, long time series snow cover datasets is urgently needed to drive  
37 hydrometeorological simulations and land surface process models. Among them, snow water equivalent (SWE) data play an  
38 irreplaceable role as an important parameter of the land surface hydrological model and climate model.

39 At present, there are many forms of SWE data in the world. According to type, these data can be divided into site  
40 observational SWE, remote sensing SWE, reanalysis SWE, data assimilation SWE and model simulation SWE. The remote  
41 sensing SWEs are mainly AMSR-E (Kelly, 2009) and AMSR2 (Imaoka et al., 2010; Tedesco and Jeyaratnam, 2019). The  
42 reanalysis SWE was mainly based on the ERA-Interim (Dee et al., 2011), MERRA2 (Gelaro et al., 2017), MERRA land  
43 (Reichle et al., 2011), and ERA5-land (Muñoz Sabater, 2019; Balsamo et al., 2015) datasets. The data assimilation SWE  
44 mainly includes GlobSnow (Luoju et al., 2021) and Global Land Data Assimilation System (GLDAS) (Rodell et al., 2004).  
45 The site observational SWE mainly includes the GHCN dataset (Menne et al., 2016) and HSSC data (Pulliainen et al., 2020).  
46 However, the time ranges of AMSR-E and AMSR-E2 SWE are only from 2003 to present, which is lacking in terms of time  
47 series. Similarly, the GlobSnow SWE dataset is also seriously lacking in time series. Although the reanalysis SWE data have

48 good spatial and temporal continuity and high data integrity, their accuracy is poor, and the MAE is 0.65 (Snauffer et al.,  
49 2016). The SWE data from stations and meteorological observations cannot meet the needs of hydrometeorological and  
50 climate change research. This is mainly because SWE from stations is discontinuous in time series and severely missing.  
51 Furthermore, hydrometeorological studies often require spatiotemporally continuous grid data to be derived (Pan et al.,  
52 2003). There are great differences among remote-sensing SWE, reanalysis SWE data, data assimilation SWE and  
53 observational SWE. For remote-sensing SWE, the spatiotemporal characteristics of different passive microwave SWE data  
54 differ significantly due to differences in sensors or retrieval algorithms (Mudryk et al., 2015a). Data assimilation SWE and  
55 reanalysis SWE data also tend to exhibit different spatiotemporal characteristics due to differences in model design, driving  
56 data, and assimilation methods (Vuyovich et al., 2014). In summary, although there are a variety of SWE data in the world,  
57 the data quality is uncertain.

58 Previous studies have shown that all kinds of SWE data in the Northern Hemisphere have advantages and disadvantages,  
59 and none of these data perform well in all aspects (Mortimer et al., 2020). An effective method was applied in a study by  
60 Pulliainen et al (Pulliainen et al., 2020), who applied a bias correction to GlobSnow and reanalysis data products based on  
61 SWE snow course measurements to obtain improved estimates on annual peak snow mass and SWE in the Northern  
62 Hemisphere. Another effective method is to fuse all kinds of SWE data in time and space, integrate the advantages of all  
63 kinds of data, and then generate a relatively complete SWE dataset. Many scholars have conducted in-depth studies on SWE  
64 data fusion. The main fusion methods can be classified into the following categories: multiproduct direct average (Mudryk et  
65 al., 2015b), linear regression (Snauffer et al., 2016), data assimilation (Pulliainen, 2006), “multiple” collocation (Pan et al.,  
66 2015) and machine learning (Snauffer et al., 2018; Xiao et al., 2018; Wang et al., 2020). Studies have shown that even the  
67 simplest multisource data average is more accurate than a single SWE product (Snauffer et al., 2018). However, the simple  
68 multisource data average cannot highlight the advantages of high-precision data, and it is easily affected by the weight ratio  
69 of low-precision data, which reduces the accuracy of fused data (Mudryk et al., 2015a). Although the linear regression  
70 method can make good use of the actual observational data to correct the original data, it is easy to overfit and causes the  
71 overall deviation (Snauffer et al., 2016). The “multiple” collocation method changes the size of the original SWE data before  
72 fusion, which easily causes data errors. The data assimilation method is sensitive to the accuracy of input data, and it is

73 difficult to fuse multisource data (Pan et al., 2015). In recent years, machine learning methods have been widely used in data  
74 fusion (Santi et al., 2021; Ntokas et al., 2021). Machine learning methods can not only integrate the advantages of  
75 multisource data but also make full use of site observational data to train the sample data, which easily generates SWE data  
76 products with large spatial scales and long time series (Broxton et al., 2019; Bair et al., 2018).

77 In summary, based on the existing SWE data products, combining a machine learning algorithm to fuse multisource SWE  
78 data is an effective method to prepare SWE products with long time series and large spatial scales and retain the advantages  
79 of single SWE data products. The ridge regression model is a biased estimation method specifically designed to address the  
80 problem of multicollinear data (Duzan and Shariff, 2015; Saleh et al., 2019). It has good tolerance to "ill-conditioned" data  
81 and has a good effect in using SWE data to address the multicollinearity problem (Hoerl and Kennard, 1970b; Guilkey and  
82 Murphy, 1975). In this study, we integrated multisource SWE data products of the RRM SWE based on the ridge regression  
83 model of the machine learning algorithm. We selected ERA-Interim SWE, GLDAS SWE, GlobSnow SWE, AMSR-  
84 E/AMSR2 SWE, and ERA5-land SWE data with relatively complete time series as the original data for the production of the  
85 RRM SWE product. The missing parts of the ERA-Interim SWE, AMSR-E/AMSR2 SWE, and GlobSnow SWE data were  
86 filled by the spatiotemporal interpolation method. The HSSC dataset (Pulliainen et al., 2020) and Russian snow survey data  
87 (Bulygina et al., 2011) were used as training sample data of "true SWE", and the effect of altitude on the algorithm was also  
88 considered. Thus, we prepared a set of spatiotemporal seamless SWE datasets (RRM SWE) covering the land region above  
89 45° N from 1979 to 2019. The spatial coverage of the RRM SWE product covers all land regions north of 45° N.

## 90 **2 Data and methods**

### 91 **2.1 Research region**

92 The research region of the RRM SWE product is located in the land region north of 45° N (Fig. 1). This region consists of  
93 Asia, Europe, and North America. The land region covers Russia, the United States, Canada, Denmark, Norway, Iceland,  
94 Sweden, and Finland. This region has a cold climate and a wide area of snow cover.

## 95 2.2 Grid SWE data description

96 In this study, we utilized ERA-Interim SWE data (Dee et al., 2011), GLDAS SWE data (Rodell et al., 2004), GlobSnow  
97 SWE data (Luoju et al., 2021), AMSR-E/AMSR2 SWE data (Tedesco and Jeyaratnam, 2019), and ERA5-land SWE data  
98 (Muñoz Sabater, 2019) as the original input datasets for the fusion data (Table 1).

99 GlobSnow is a dataset of global snow cover and SWEs for the Northern Hemisphere released by the European Space  
100 Agency (ESA) (<http://www.globsnow.info/swe/>) (Luoju et al., 2021; Pulliainen et al., 2020). The SWE products in this  
101 dataset combine the Canadian Meteorological Center (CMC) daily snow depth analysis data (Walker et al., 2011), ground  
102 weather site observational data, and satellite microwave radiometer data. We obtained the L3A\_daily\_SWE product of this  
103 dataset. The temporal resolution of the L3A\_daily\_SWE product is daily, the spatial resolution is  $0.25^\circ$ , and the data format  
104 is NETCDF4.

105 ERA-Interim is the fourth generation reanalysis data of the European Centre for Medium-Range Weather Forecasts  
106 (ECMWF) (Dee et al., 2011). The data provide a global assimilated numerical product of various surface and top  
107 atmospheric parameters from January 1979 to present (<https://apps.ecmwf.int/datasets/data/interim-full-daily/levtype=sfc/>).  
108 We obtained the SWE dataset with a daily temporal resolution, a spatial resolution of  $0.25^\circ$ , and NETCDF4 data format. The  
109 spatial range of the data is the land region above  $45^\circ$  N.

110 The Advanced Microwave Scanning Radiometer-Earth Observing System (AMSR-E) is a microwave scanning  
111 radiometer on the Aqua satellite of the National Aeronautics and Space Administration (NASA) Earth Observing System  
112 (EOS) (Tedesco and Jeyaratnam, 2019). The AMSR-E provides a global daily SWE dataset from June 19, 2002, to October  
113 3, 2011 ([https://nsidc.org/data/ae\\_dysno](https://nsidc.org/data/ae_dysno)). AMSR2 is a microwave scanning radiometer on the GCOM-W1 satellite launched  
114 by the Japan Aerospace Exploration Agency (JAXA) in May 2012. AMSR2 provides a global SWE dataset from July 2,  
115 2012, to the present ([https://nsidc.org/data/AU\\_DySno/versions/1](https://nsidc.org/data/AU_DySno/versions/1)). The spatial resolution of the AMSR-E SWE and AMSR2  
116 SWE datasets is 25 km x 25 km, the temporal resolution is daily, and the data formats are HDF-EOS and HDF-EOS5,  
117 respectively.

118 The GLDAS is a model used to describe global land information; it contains data, such as global rainfall, water  
119 evaporation, surface runoff, underground runoff, soil moisture, surface snow cover distribution, temperature, and heat flow

120 distribution (Rodell et al., 2004). This assimilation system includes data with spatial resolutions of  $1^{\circ}\times 1^{\circ}$  and  $0.25^{\circ}\times 0.25^{\circ}$   
121 and temporal resolutions of 3 hours, 1 day and 1 month. The GLDAS data are available for download from the Goddard  
122 Earth Sciences Data and Information Services Center (GES DISC). We obtain an SWE dataset with the daily temporal  
123 resolution,  $0.25^{\circ}$  spatial resolution, and NETCDF4 data format.

124 ERA5-land is a reanalysis dataset that provides the evolution of global land parameter data since 1981 (Muñoz Sabater,  
125 2019). The dataset provides eight types of snow parameter data, including snow albedo, snow cover, snow depth, snowfall,  
126 the temperature of the snow layer, snowmelt, snow density, and SWE. This dataset provides a global SWE dataset with an  
127 hourly spatial resolution, a temporal resolution of  $0.1^{\circ}\times 0.1^{\circ}$ , a temporal coverage of January 1981 to the present, and data  
128 formats of GRIB and NETCDF4.

129 To maintain consistency in the spatial and temporal resolutions of the fused data, we unified the ERA-Interim SWE data,  
130 GLDAS SWE data, GlobSnow SWE data, AMSR-E/AMSR2 SWE data, and ERA5-land SWE data into a daily temporal  
131 resolution, with a spatial resolution of  $0.25^{\circ}$  and geographic projection of North Pole Lambert Azimuthal Equal Area.

### 132 **2.3 Ridge regression machine learning algorithm for preparing the SWE**

133 In this study, we utilize the ridge regression model of a machine learning algorithm to fuse ERA-Interim SWE data (Dee et  
134 al., 2011), GLDAS SWE data (Rodell et al., 2004), GlobSnow SWE data (Luo et al., 2021), AMSR-E/AMSR2 SWE data  
135 (Tedesco and Jeyaratnam, 2019), and ERA5-land SWE data (Muñoz Sabater, 2019) to generate a set of new RRM SWE  
136 datasets. The target reference data in this study are the HSSC dataset and Russian snow survey data. The digital elevation  
137 model (DEM) was used as an important environmental feature input to the ridge regression model and was included in the  
138 model training. The DEM is an auxiliary terrain feature variable in addition to the five SWE prediction feature variables,  
139 AMSR-E/AMSR2 SWE, ERA-Interim SWE, GLDAS SWE, GlobSnow SWE, and ERA5-land SWE.

140 The ridge regression model is a biased estimates regression method for collinear data analysis (Friedman et al., 2010;  
141 Hoerl and Kennard, 1970b, a). By abandoning the unbiasedness of the ordinary least squares, this algorithm can obtain the  
142 regression method in which the regression coefficient is more practical and reliable at the cost of losing part of the  
143 information and reducing the accuracy. The ridge regression model is flexible in the choice of predictor variables and does

144 not require the predictor and target variable to be independent of each other. It can effectively solve the multicollinearity  
 145 problem of predictor and target variables as well as reduce the impact of this problem on the training model (Duzan and  
 146 Shariff, 2015; Saleh et al., 2019). Generally, since the reanalysis data based on SWE products cannot make the products and  
 147 models independent of each other, i.e., they are prone to the multicollinearity problem, which leads to distorted model  
 148 estimation or difficulty in performing accurate estimations. In contrast, the ridge regression model can successfully solve the  
 149 multicollinearity problem, i.e., the independence of training products and models. In addition, when integrating multiple  
 150 SWE products, the accuracy of each SWE dataset is likely to differ. A small change in one of the SWE products involved in  
 151 the training will cause a significant error in the final calculation results, while the ridge regression model has high accuracy  
 152 and stability for this "ill-conditioned" SWE data. In addition, the main advantage of this model is that SWE products with  
 153 long time series and large spatial scales are easy to prepare. The principle equation of the ridge regression model is defined  
 154 as follows:

$$155 \quad \hat{\beta}^{ridge} = \underset{\beta}{\operatorname{argmin}} \left\{ \sum_{i=1}^N \left( y_i - \beta_0 - \sum_{j=1}^p x_{ij} \beta_j \right)^2 + \lambda \sum_{j=1}^p \beta_j^2 \right\}, \quad (1)$$

156 where  $\hat{\beta}^{ridge}$  is the extremum solution function of ridge regression and  $p$  is the number of gridded SWE product variables  
 157 involved in training.  $x_i$  are the prediction feature variables, which contain two parts, one set contains the main feature  
 158 variables of the gridded SWE products, and the other part consists of the DEM auxiliary feature variables.  $y_i$  is the observed  
 159 SWE, and  $\lambda$ ,  $\beta$ ,  $\beta_j$  and  $\beta_0$  are the parameters to be solved.  $1, \dots, N$  is the sample of the training dataset.  $\lambda \sum_{j=1}^p \beta_j^2$  is the  
 160 penalty function terms. The total number of samples  $N$  in the training dataset is 271651. The sample sizes of the training  
 161 data set, validation data set and test data set are divided according to the ratio of 7:2:1, where the numbers of training set,  
 162 validation set and test set samples are 271651, 77614 and 38807, respectively. The model is developed in python3, and the  
 163 model framework is based on the "scikit-learn" machine learning library (<https://scikit-learn.org/stable/index.html>). The code  
 164 is available upon request.

165 The integration process of the RRM SWE product (Fig. 2) is described as follows:

- 166 1) The original ERA-Interim SWE data, GLDAS SWE data, GlobSnow SWE data, AMSR-E/AMSR2 SWE data, ERA5-  
167 land SWE data, DEM data, unified temporal resolution, spatial resolution, projection, spatial range, and unit are  
168 preprocessed.
- 169 2) The spatiotemporal interpolation method is used to fill in the missing data of AMSR-E/AMSR2 SWE, ERA-Interim  
170 SWE, and GlobSnow SWE in space and time. Based on this method, the missing data of AMSR-E/AMSR2 SWE at  
171 low latitudes and the missing data of ERA-Interim SWE and GlobSnow SWE in the time series are added.
- 172 3) The SWE data observed at stations from 1979 to 2014 are used as sample training data, and the AMSR-E/AMSR2  
173 SWE, ERA-Interim SWE, GLDAS SWE, GlobSnow SWE, ERA5-land SWE data, and DEM data are input into the  
174 ridge regression model of a machine learning algorithm for training. During the model training process, we restructured  
175 the training data, reduced the training data appropriately for the regions with denser training data, selected the sample  
176 points that were spatially uniformly distributed for training as much as possible based on the latitude and longitude  
177 information of the observational points, and made the amount of training data in the denser region close to the amount  
178 of training data in the sparse region.
- 179 4) When the model was trained, ERA-Interim SWE, GLDAS SWE, GlobSnow SWE, and ERA5-land SWE were used as  
180 the training data between 1979 and 2002 (AMSR-E/AMSR2 SWE data were not available before 2002), and AMSR-  
181 E/AMSR2 SWE, ERA-Interim SWE, GLDAS SWE, GlobSnow SWE, and ERA5-land SWE were used as the training  
182 data after 2002.
- 183 5) Based on the S-fold cross-validation method, the SWE data are continuously trained and validated, and the optimal  
184 model and parameters are finally selected and evaluated by the loss function.
- 185 6) Based on the trained optimal model, multiple SWE data products are integrated into the time series, missing data are  
186 predicted, and a set of spatiotemporally seamless SWE datasets is generated.
- 187 7) SWE data observed at stations from 2015 to 2018 are used to evaluate the accuracy of the RRM SWE product.



## 188 2.4 Site data and evaluation metrics

### 189 2.4.1 Site SWE data for training, validation, and testing

190 Russian snow survey data (<http://aisori.meteo.ru/ClimateR>) include the average snow depth data and the average snow  
191 density data of the station, and the SWE is the product of the measured average snow depth and average snow density  
192 (Bulygina et al., 2011). We obtained the SWE data of 19493 stations in 1979-2016 from this dataset.

193 Hemispheric-scale snow course (hereinafter referred to as HSSC) observational data are contained in a hemispheric-scale  
194 SWE database based on SWE observational datasets from the former Soviet Union/Russia (FSU), Finland, and Canada  
195 developed by Pulliainen et al (Pulliainen et al., 2020; Bronnimann et al., 2018; Brown et al., 2019). This dataset is from the  
196 website of the Finnish Meteorological Institute (FMI) ([https://www.globsnow.info/swe/archive\\_v3.0/auxiliary\\_data/](https://www.globsnow.info/swe/archive_v3.0/auxiliary_data/)). The  
197 dataset provides data from 2687 distributed regional snow course observations and contains 343,241 SWE observational data  
198 points from 1979 to 2018. The dataset is a manually sampled transect, which can effectively solve the problem of spatial  
199 scale uncertainty of SWE observational data.

200 We carefully screened the Russian snow survey data and HSSC data and eliminated some abnormal observational data to  
201 ensure the high quality of the training, validation, and test sets. The null and zero values are removed during the HSSC data  
202 screening process. The null values, negative numbers, and extreme SWE values greater than 2000 mm are removed during  
203 the Russian snow survey data screening process.

### 204 2.4.2 Accuracy evaluation method for datasets

205 Mean absolute error (MAE), root mean square error (RMSE), Pearson's correlation coefficient (R), and coefficient of  
206 determination ( $R^2$ ) are used to evaluate the accuracies of AMSR-E/AMSR2 SWE, ERA-Interim SWE, GLDAS SWE,  
207 GlobSnow SWE, ERA5-land SWE, multisource data-averaged SWE, and the RRM SWE product. The specific equation of  
208 accuracy evaluation error is described as follows.

$$209 \quad MAE = \frac{1}{n} \sum_{i=1}^n |f_i - y_i|, \quad (2)$$

$$210 \quad RMSE = \left[ \frac{\sum_{i=1}^n (f_i - y_i)^2}{n} \right]^{\frac{1}{2}}, \quad (3)$$

$$211 \quad R = \frac{1}{n-1} \sum_{i=1}^n \left( \frac{f_i - \bar{f}}{\sigma_f} \right) \left( \frac{y_i - \bar{y}}{\sigma_y} \right), \quad (4)$$

$$212 \quad R^2 = \frac{\sum_{i=1}^n (f_i - \bar{f})^2}{\sum_{i=1}^n (y_i - \bar{y})^2}, \quad (5)$$

213 where  $n$  is the number of samples in the validation dataset,  $f_i$  is the SWE dataset product, and  $y_i$  is the measured SWE at  
 214 the station.  $\bar{f}$  and  $\bar{y}$  are the averages of SWE products and measured SWEs, respectively.  $\sigma_f$  and  $\sigma_y$  are the standard  
 215 deviation of SWE products and measured SWEs, respectively.

216 To further evaluate the accuracy of the RRM SWE dataset at the spatial scale, we compared it with AMSR-E/AMSR2  
 217 SWE, ERA-Interim SWE, GLDAS SWE, GlobSnow SWE, and ERA5-Land SWE at different altitude gradients. We also  
 218 evaluated MAE, RMSE, R and  $R^2$  separately for 11 elevation intervals: <100 m, 100-200 m, 200-300 m, 300-400 m, 400-  
 219 500 m, 500-600 m, 600-700 m, 700-800 m, 800-900 m, 900-1000 m, and >1000 m. In addition, we evaluated the  
 220 performances of the RRM SWE product in three representative regions: Russia, Canada, and Finland.

221 We used the Mann-Kendall trend test (Mann, 1945; Kendall, 1990) method to evaluate the variation trend in the RRM  
 222 SWE dataset from 1979 to 2019 and analyzed its reliability in terms of time series. Since the AMSR-E/AMSR2 SWE  
 223 product and the GlobSnow SWE product lacked SWE data for Greenland, we removed the Greenland data to maintain  
 224 consistency in the spatial extent of the comparison data.

## 225 **3 Results and discussion**

### 226 **3.1 Overall accuracy evaluation of the RRM SWE product**

227 In this study, the accuracy of the RRM SWE, AMSR-E/AMSR2 SWE, ERA-Interim SWE, GLDAS SWE, GlobSnow SWE,  
228 and ERA5-land SWE was compared using test datasets from 2015 to 2018. MAE, RMSE, R, and  $R^2$  were used to reflect the  
229 data quality of each SWE product. In addition, we compared the RRM SWE product with the SWE dataset obtained by the  
230 multisource data average method.

231 According to the verification results in Fig. 3 and Table 2, the RRM SWE data have the best overall accuracy, and the  
232 MAE, RMSE, R, and  $R^2$  between the observed SWEs are 0.21, 25.37 mm, 0.89, and 0.79, respectively. The overall accuracy  
233 of the GlobSnow SWE and ERA5-land SWE products is higher than that of other SWE products. The overall deviation of  
234 the ERA5-land SWE products is the smallest except for the RRM SWE data, with MAE and RMSE values of 0.32 and 37.02  
235 mm, respectively. The correlation between the ERA5-land SWE and observed SWE is the highest except for the RRM SWE  
236 data, with R and  $R^2$  values of 0.84 and 0.71, respectively. Although the overall deviation between the GlobSnow SWE  
237 dataset and the measured SWE is small, its correlation with the measured value is low. The overall deviation between the  
238 ERA5-land SWE dataset and the measured SWE is higher than that of the GlobSnow SWE dataset, but its estimation  
239 accuracy for the high-value region of the SWE is low. In addition, the overall accuracy of the ERA-Interim SWE dataset and  
240 GLDAS SWE dataset is relatively low, but their integrities are higher than that of the GlobSnow SWE dataset and AMSR-  
241 E/AMSR2 SWE dataset in terms of temporal and spatial series. The AMSR-E/AMSR2 SWE dataset has a higher estimation  
242 accuracy for the low-value region of SWE. Moreover, in the land region above 45° N, most of the existing SWE data  
243 products with regard to temporal and spatial degrees are missing to various degrees. Obviously, the accuracies of the existing  
244 SWE products were uneven, and no type of SWE dataset is absolutely perfect.

245 The verification results also indicate the following ranking orders:

246 The MAE ranking order is RRM SWE < GlobSnow SWE = ERA5-land SWE < ERA-Interim SWE < multisource data  
247 average SWE < AMSR-E/AMSR2 SWE < GLDAS SWE.

248 The RMSE ranking order is RRM SWE < ERA5-land SWE < GlobSnow SWE < ERA-Interim SWE < multisource data

249 average SWE < AMSR-E/AMSR2 SWE < GLDAS SWE.

250 The R ranking order is RRM SWE > ERA5-land SWE > GlobSnow SWE > ERA-Interim SWE > GLDAS SWE >  
251 multisource data average SWE > AMSR-E/AMSR2 SWE.

252 The R<sup>2</sup> ranking order is RRM SWE > ERA5-land SWE > GlobSnow SWE > ERA-Interim SWE > GLDAS SWE >  
253 multisource data average SWE > AMSR-E/AMSR2 SWE.

254 Compared with ERA-Interim SWE, AMSR-E/AMSR2 SWE, GLDAS SWE, GlobSnow SWE, ERA5-land SWE, and  
255 multisource data average SWE, the MAE of the RRM SWE and observed SWE is reduced by 0.22, 0.28, 0.37, 0.11, 0.11 and  
256 0.23, respectively. The RMSE of the RRM SWE and observed SWE is reduced by 21.44 mm, 27.02 mm, 39.88 mm, 15.62  
257 mm, 11.65 mm, and 26.63 mm, respectively. The correlation coefficient of the RRM SWE and observed SWE is improved  
258 by 0.20, 0.42, 0.37, 0.19, 0.05, and 0.38, respectively. The coefficient of determination of the RRM SWE and observed SWE  
259 is improved by 0.31, 0.57, 0.52, 0.30, 0.08, and 0.53, respectively. Although the multisource data average method can  
260 improve the accuracy of SWE products to some extent (better than AMSR-E/AMSR2 SWE and GLDAS SWE), the  
261 improvement of this method is still very limited. The RRM SWE product has a significant advantage over the multisource  
262 data average method, and its accuracy is much higher than that of the simple multisource data average method. Based on the  
263 above verification results, the accuracy of the RRM SWE is significantly improved; the RRM SWE dataset has higher  
264 accuracy than that of any single grid SWE dataset, and it also fills the gap in the original SWE data in terms of spatial and  
265 temporal resolutions.

266 Based on the kernel density estimation method, we analyzed the density distribution of different SWE datasets (Fig. 4).  
267 The results show that the RRM SWE dataset is closer to the 1:1 line and has the highest accuracy. The RRM SWE dataset is  
268 particularly accurate for SWE estimation in the low-value region, and the test data are concentrated near the 1:1 line in the  
269 high-density region (kernel density estimation > 0.00015) (Fig. 4). In contrast, the high-density regions of the GLDAS SWE  
270 dataset, ERA-Interim SWE dataset, and AMSR-E/AMSR2 SWE dataset deviate significantly from the 1:1 line, resulting in  
271 poor accuracy. The AMSR-E/AMSR2 SWE, GLDAS SWE, and GlobSnow SWE are underestimated relative to the SWE  
272 measured at the site, among which GLDAS SWE underestimated the observed SWE the most seriously, while ERA5-land  
273 SWE overestimated the observed SWE. Although the accuracies of GlobSnow SWE and ERA5-land SWE are relatively

274 high, their dispersion degrees are large (the kernel density estimation for most test data is less than 0.0001). Overall, the  
275 RRM SWE data have a higher overall estimation accuracy, especially for the low-value area of SWE. For an SWE above  
276 400 mm, the MAE and RMSE of the RRM SWE product and the measured SWE are 0.35 and 43.57 mm, respectively.  
277 Although the RRM SWE product is better than other products at capturing the SWE above 400 mm, it is still not as good at  
278 capturing the SWE below 400 mm relative to itself.

279 However, in this study, there are still some uncertainties in the ridge regression machine learning algorithm that integrates  
280 SWE products. First, this model is strongly dependent on on-site observational data, and the fusion precision of SWE is poor  
281 in some areas with sparse observational stations. The fusion accuracy of SWE products will be affected to a certain extent  
282 without considering the prior snow cover information. The RRM SWE product is still underestimated in cases of high SWE.  
283 Then, in addition to the DEM, meteorological elements, NDVI, land type, and other factors will affect the SWE estimation.  
284 Unfortunately, our current training model does not consider these factors in detail, which is a limitation of the current RRM  
285 SWE product. Finally, in complex terrain, the integration of SWE products remains challenging.

### 286 **3.2 Accuracy evaluation of the RRM SWE product at different altitudes and regions**

287 The accuracy of each SWE product is not absolute at different altitude gradients based on evaluations of the AMSR-  
288 E/AMSR2 SWE, ERA-Interim SWE, GLDAS SWE, GlobSnow SWE, and ERA5-land SWE products' accuracies (Fig. 5).  
289 The accuracy of a single SWE product is different from its overall accuracy. We consider the influence of altitude in the  
290 algorithm and make full use of the accuracy advantage of each SWE data for different altitude gradients.

291 The above verification results show that the MAEs between the RRM SWE dataset and measured SWE are 0.16, 0.21,  
292 0.24, 0.23, 0.22, 0.18, 0.23, 0.19, 0.29, 0.27, and 0.18; the RMSEs are 5 mm, 21 mm, 27 mm, 25 mm, 25 mm, 12 mm, 9 mm,  
293 6 mm, 28 mm, 29 mm, and 31 mm; the R values are 0.97, 0.88, 0.88, 0.82, 0.85, 0.96, 0.88, 0.84, 0.90, 0.81, and 0.83; and  
294 the  $R^2$  values are 0.95, 0.77, 0.78, 0.67, 0.73, 0.91, 0.77, 0.70, 0.81, 0.66, and 0.70 at altitude gradients of <100 m, 100-200  
295 m, 200-300 m, 300-400 m, 400-500 m, 500-600 m, 600-700 m, 700-800 m, 800-900 m, 900-1000 m and >1000 m,  
296 respectively (Fig. 5). Overall, the RRM SWE product has the highest accuracy in the elevation intervals of <100 m, 100-200  
297 m, 200-300 m, 400-500 m, 500-600 m, 600-700 m, 700-800 m, 800-900 m, and >1000 m. For the RRM SWE product itself,

298 it has the best performance in the elevation interval <100 m. The ERA5-land product has the best performance in the  
299 elevation interval 300-400 m. The GlobSnow product has the best performance in the elevation interval 900-1000 m.

300 RRM SWE product has good performance in different regions, and its RMSE in Russia, Canada, and Finland are 26.39  
301 mm, 29.31 mm, and 25.29 mm, respectively; additionally, the performance of the RRM SWE product in different regions is  
302 basically similar (Table 3). The RRM SWE product performs well not only at different altitudes but also in different regions,  
303 and it has good stability.

### 304 **3.3 Comparison of spatial distribution patterns between the RRM SWE product and traditional SWE products**

305 A comparison of the spatially distributed annual average SWE distributions is made between the RRM SWE and AMSR-  
306 E/AMSR2 SWE, ERA-Interim SWE, GLDAS SWE, GlobSnow SWE, and ERA5-land SWE in 2014, 2015, 2016, and 2017,  
307 and their spatial distribution patterns are shown in Fig. 6.

308 Overall, the RRM SWE dataset, AMSR-E/AMSR2 SWE dataset, ERA-Interim SWE dataset, GLDAS SWE dataset,  
309 GlobSnow SWE dataset, and ERA5-land SWE dataset have similar spatial distribution patterns in the land region above 45°  
310 N, showing a trend of lower SWE in low latitudes and higher SWE in high latitudes. The AMSR-E/AMSR2 SWE dataset  
311 covers a limited extent in the land region above 45° N, many data points are missing, and low SWE values exist at low  
312 latitudes. In northern Siberia, the ERA-Interim SWE product has a higher SWE, and there are many abnormal, extreme SWE  
313 values (SWE > 500 mm) in this dataset. In low-latitude regions, such as Alaska, North Siberia, and the easternmost region of  
314 Russia, the SWE of GLDAS SWE products is significantly lower. The GlobSnow SWE product lacks SWE data for  
315 Greenland, and this dataset has low SWEs in the Baffin Island, the Koryak Mountains, the Kamchatka Peninsula, and Alaska  
316 regions. The ERA5-land SWE products have low SWEs in northeastern Russia, Scandinavia, and northeastern Canada. The  
317 RRM SWE dataset is more reasonable for estimating the spatial distribution of SWE in the land region above 45° N, and the  
318 data integrity is higher. Moreover, based on the new machine learning algorithm, a variety of SWE data products in different  
319 time series are fused, which makes the RRM SWE dataset completely temporally and spatially continuous.

320 The relative difference between the RRM SWE data and GLDAS SWE data is the highest, and the relative difference is  
321 greater than 80% in most low altitude regions (Fig. 7). The relative difference between the RRM SWE data and the

322 GlobSnow SWE data is relatively small overall, especially in most high-latitude areas where the relative difference is less  
323 than 10% (Fig. 7). Overall, the annual average relative differences in the RRM SWE data and AMSR2 SWE, ERA-Interim  
324 SWE, GLDAS SWE, GlobSnow SWE, and ERA5-land SWE are 37%, 41%, 54%, 25%, and 29%, respectively (Fig. 7).  
325 Previous studies have shown that the accuracy of the SWE in the Northern Hemisphere estimated by GlobSnow SWE data is  
326 higher (Pulliainen et al., 2020), while the spatial distribution pattern of the RRM SWE data is close to the estimation result of  
327 GlobSnow SWE. In addition, the single point verification results based on the measured SWE data of meteorological stations  
328 in section 3.1 show that the RRM SWE dataset has higher accuracy than the GlobSnow SWE dataset. The RRM SWE  
329 dataset has good accuracy.

### 330 **3.4 Comparison of the annual variation tendencies of AMSR-E/AMSR2 SWE, ERA-Interim SWE, GLDAS SWE,** 331 **GlobSnow SWE, and ERA5-land SWE and the RRM SWE in the land region above 45° N**

332 Based on the Mann-Kendall trend test, we analyzed the changing trend in the region-wide annual average SWE of the  
333 AMSR-E/AMSR2 SWE, ERA-Interim SWE, GLDAS SWE, GlobSnow SWE, ERA5-land SWE, and RRM SWE in the land  
334 region above 45° N from 1979 to 2019.

335 Based on the Mann-Kendall trend test (see Fig. 8 and Table 4), from 1979 to 2019, the test value of the ERA-Interim  
336 region-wide annual average SWE is 1.08, and there is no significant change trend under the significance test level of 0.05.  
337 The test value of the GLDAS region-wide annual average SWE was 4.95 and showed a significant increasing trend at the  
338 significance test level of 0.05. The test values of the AMSR-E/AMSR2 annual average SWE, GlobSnow annual average  
339 SWE, ERA5-land annual average SWE, and RRM annual average SWE are -3.26, -2.54, -3.43, and -3.00, respectively, and  
340 these four SWEs showed a significantly decreasing trend at the significance test level of 0.05. Based on the analysis of the  
341 RRM SWE product, between 1979 and 2019, the region-wide annual average SWE in the land region above 45° N decreased  
342 by 15.1 percent. In the Northern Hemisphere, spring snow cover extent has decreased significantly, according to the Fifth  
343 Assessment Report (AR5) of the IPCC. Between 1967 and 2010, the spring snow cover extent decreased by an average of  
344 1.6 percent per decade, while the June snow cover extent decreased by 11.7 percent per decade (Stocker, 2014). Most studies  
345 have shown that the annual variation tendency of snow depth and snow cover extent showed a significant decreasing trend in

346 the Northern Hemisphere (Brutel-Vuilmet et al., 2013), which is consistent with the annual variation tendency of the RRM  
347 SWE dataset. This dataset can reflect the characteristics of snow cover change in the land region above 45° N under the  
348 background of climate change and can be used as the driving data for the climate model to support climate change-related  
349 research. In addition, this dataset is expected to provide a snow data basis for the study of "Arctic amplification".

#### 350 **4 Data availability**

351 The RRM SWE product is available for free download from ‘A Big Earth Data Platform for Three Poles’  
352 (<http://dx.doi.org/10.11888/Snow.tpd.271556>) (Li et al., 2021). The temporal resolution of the RRM SWE product is daily,  
353 and the spatial resolution is 10 km. It spans latitudes of 45°N-90°N and longitudes of 180°W-180°E. A brief summary and  
354 data description document (including data details, spatial range, and usage method) are also provided.

#### 355 **5 Conclusions**

356 In this study, we propose a method to fuse multisource SWE data by a ridge regression model based on machine learning. A  
357 new method was utilized to prepare a set of spatiotemporal seamless SWE datasets of the RRM SWE, combined with the  
358 original AMSR-E/AMSR2 SWE, ERA-Interim SWE, GLDAS SWE, GlobSnow SWE, and ERA5-land SWE datasets. In the  
359 RRM SWE dataset, the time series of the data is 1979-2019, the temporal resolution is daily, the spatial resolution is 10 km,  
360 and the spatial range is the land region above 45° N.

361 The RRM SWE data product has the best accuracy, especially for the estimation of low SWE. The accuracy ranking of the  
362 SWE dataset verified by the test dataset is described as follows: RRM SWE > ERA5-land SWE > GlobSnow SWE > ERA-  
363 Interim SWE > multisource data average SWE > AMSR-E/AMSR2 SWE > GLDAS SWE. The accuracy of the RRM SWE  
364 dataset is higher than that of the existing SWE products at most elevation intervals. The RRM SWE product has good  
365 performance and stability in different regions. Moreover, the RRM SWE dataset fills in the missing data of the original SWE  
366 dataset spatiotemporally.

367 Compared with traditional fusion methods, machine learning methods have a good advantage. We find that the simple



368 machine learning algorithm has not only high efficiency but also good accuracy in the preparation of SWE products on a  
369 global scale. Without losing the advantages of existing SWE products, this method can also make full use of station  
370 observational data to integrate the advantages of various SWE products. The model training process does not rely too much  
371 on a specific sample, and this model has a strong generalization ability. In addition, the influence of altitude on the  
372 preparation scheme is considered in detail in the model. Compared with the SWE dataset prepared by the traditional method,  
373 the spatial resolution is only 25 km, while this new method obtains an SWE dataset with a higher spatial resolution of 10 km.

374 We propose that the RRM SWE dataset preparation scheme has good continuity and can prepare real-time and high-  
375 quality SWE datasets in the land region above 45° N. In addition, the new method proposed in this paper has the advantages  
376 of simplicity and high precision in preparing large-scale SWE datasets and can be easily extended to the preparation of other  
377 snow datasets. This dataset is an important supplement to the land region above 45° N SWE database and is expected to  
378 provide data support for Arctic cryosphere studies and global climate change studies.

#### 379 **Author contributions.**

380 DS and HL designed the study and wrote the manuscript; JW, XH, and TC contributed to the discussions, edits, and  
381 revisions. DS and WJ compiled the model code.

#### 382 **Competing interests.**

383 The authors declare that they have no conflicts of interest.

#### 384 **Acknowledgements.**

385 The authors would like to thank the European Space Agency (ESA) for providing the GlobSnow data, the European Centre  
386 for Medium-Range Weather Forecasts (ECMWF) for ERA-Interim data and ERA5-land data, the National Aeronautics and  
387 Space Administration (NASA) for the AMSR-E/AMSR2 data, the Goddard Earth Sciences Data and Information Services  
388 Center (GESDISC) for the GLDAS data, the Russian Federal Service For Hydrometeorology and Environmental Monitoring

389 (ROSHYDROMET) for the snow survey data, and the Finnish Meteorological Institute (FMI) for the hemispheric-scale  
390 snow course (HSSC) observational data.

### 391 **Financial support.**

392 This research was supported by the Strategic Priority Research Program of the Chinese Academy of Sciences (Grant No.  
393 XDA19070302), the National Science Fund for Distinguished Young Scholars (Grant No. 42125604), and the National  
394 Natural Science Foundation of China (Grant No. 41971399, 41971325, 42171391).

### 395 **References**

396 Bair, E. H., Abreu Calfa, A., Rittger, K., and Dozier, J.: Using machine learning for real-time estimates of snow water  
397 equivalent in the watersheds of Afghanistan, *The Cryosphere*, 12, 1579-1594, 2018.

398 Balsamo, G., Albergel, C., Beljaars, A., Boussetta, S., Brun, E., Cloke, H., Dee, D., Dutra, E., Munoz-Sabater, J.,  
399 Pappenberger, F., de Rosnay, P., Stockdale, T., and Vitart, F.: ERA-Interim/Land: a global land surface reanalysis data set,  
400 *Hydrol Earth Syst Sc*, 19, 389-407, 10.5194/hess-19-389-2015, 2015.

401 Barnett, T. P., Adam, J. C., and Lettenmaier, D. P.: Potential impacts of a warming climate on water availability in snow-  
402 dominated regions, *Nature*, 438, 303-309, 10.1038/nature04141, 2005.

403 Bintanja, R. and Andry, O.: Towards a rain-dominated Arctic, *Nat Clim Change*, 7, 263-+, 10.1038/Nclimate3240, 2017.

404 Bronnimann, S., Allan, R., Atkinson, C., Buizza, R., Bulygina, O., Dahlgren, P., Dee, D., Dunn, R., Gomes, P., John, V. O.,  
405 Jourdain, S., Haimberger, L., Hersbach, H., Kennedy, J., Poli, P., Pulliainen, J., Rayner, N., Saunders, R., Schulz, J., Sterin,  
406 A., Stickler, A., Titchner, H., Valente, M. A., Ventura, C., and Wilkinson, C.: Observations for Reanalyses, *Bulletin of the*  
407 *American Meteorological Society*, 99, 1851-1866, 10.1175/Bams-D-17-0229.1, 2018.

408 Brown, R. D., Fang, B., and Mudryk, L.: Update of Canadian historical snow survey data and analysis of snow water  
409 equivalent trends, 1967–2016, *Atmosphere-Ocean*, 57, 149-156, 2019.

410 Broxton, P. D., Van Leeuwen, W. J., and Biederman, J. A.: Improving snow water equivalent maps with machine learning of

411 snow survey and lidar measurements, *Water Resources Research*, 55, 3739-3757, 2019.

412 Brutel-Vuilmet, C., Menegoz, M., and Krinner, G.: An analysis of present and future seasonal Northern Hemisphere land  
413 snow cover simulated by CMIP5 coupled climate models, *Cryosphere*, 7, 67-80, 10.5194/tc-7-67-2013, 2013.

414 Bulygina, O. N., Groisman, P. Y., Razuvaev, V. N., and Korshunova, N. N.: Changes in snow cover characteristics over  
415 Northern Eurasia since 1966, *Environmental Research Letters*, 6, Artn 045204  
416 10.1088/1748-9326/6/4/045204, 2011.

417 Dee, D. P., Uppala, S. M., Simmons, A., Berrisford, P., Poli, P., Kobayashi, S., Andrae, U., Balmaseda, M., Balsamo, G., and  
418 Bauer, d. P.: The ERA - Interim reanalysis: Configuration and performance of the data assimilation system, *Quarterly  
419 Journal of the royal meteorological society*, 137, 553-597, 2011.

420 Duzan, H. and Shariff, N. S. B. M.: Ridge regression for solving the multicollinearity problem: review of methods and  
421 models, *Journal of Applied Science*, 2015.

422 Friedman, J., Hastie, T., and Tibshirani, R.: Regularization Paths for Generalized Linear Models via Coordinate Descent, *J  
423 Stat Softw*, 33, 1-22, DOI 10.18637/jss.v033.i01, 2010.

424 Gelaro, R., McCarty, W., Suarez, M. J., Todling, R., Molod, A., Takacs, L., Randles, C. A., Darmenov, A., Bosilovich, M. G.,  
425 Reichle, R., Wargan, K., Coy, L., Cullather, R., Draper, C., Akella, S., Buchard, V., Conaty, A., da Silva, A. M., Gu, W., Kim,  
426 G. K., Koster, R., Lucchesi, R., Merkova, D., Nielsen, J. E., Partyka, G., Pawson, S., Putman, W., Rienecker, M., Schubert,  
427 S. D., Sienkiewicz, M., and Zhao, B.: The Modern-Era Retrospective Analysis for Research and Applications, Version 2  
428 (MERRA-2), *J Climate*, 30, 5419-5454, 10.1175/Jcli-D-16-0758.1, 2017.

429 Guilkey, D. K. and Murphy, J. L.: Directed Ridge Regression Techniques in Cases of Multicollinearity, *J Am Stat Assoc*, 70,  
430 769-775, 1975.

431 Henderson, G. R., Peings, Y., Furtado, J. C., and Kushner, P. J.: Snow-atmosphere coupling in the Northern Hemisphere, *Nat  
432 Clim Change*, 8, 954-+, 10.1038/s41558-018-0295-6, 2018.

433 Hoerl, A. E. and Kennard, R. W.: Ridge regression: applications to nonorthogonal problems, *Technometrics*, 12, 69-82,  
434 1970a.

435 Hoerl, A. E. and Kennard, R. W.: Ridge regression: Biased estimation for nonorthogonal problems, *Technometrics*, 12, 55-

436 67, 1970b.

437 Imaoka, K., Kachi, M., Fujii, H., Murakami, H., Hori, M., Ono, A., Igarashi, T., Nakagawa, K., Oki, T., Honda, Y., and  
438 Shimoda, H.: Global Change Observation Mission (GCOM) for Monitoring Carbon, Water Cycles, and Climate Change, P  
439 Ieee, 98, 717-734, 10.1109/Jproc.2009.2036869, 2010.

440 IPCC, 2021: Climate Change 2021: The Physical Science Basis. Contribution of Working Group I to the Sixth Assessment  
441 Report of the Intergovernmental Panel on Climate Change [Masson-Delmotte, V., P. Zhai, A. Pirani, S.L. Connors, C. Péan,  
442 S. Berger, N. Caud, Y. Chen, L. Goldfarb, M.I. Gomis, M. Huang, K. Leitzell, E. Lonnoy, J.B.R. Matthews, T.K. Maycock,  
443 T. Waterfield, O. Yelekçi, R. Yu, and B. Zhou (eds.)]. Cambridge University Press. In Press.

444 Kelly, R.: The AMSR-E Snow Depth Algorithm: Description and Initial Results, 2009.

445 Kendall, M. G.: Rank Correlation Methods, *British Journal of Psychology*, 25, 86–91, 1990.

446 Li, H., Shao, D., Li, H., Wang, W., Ma, Y., and Lei, H.: Arctic Snow Water Equivalent Grid Dataset (1979-2019), A Big  
447 Earth Data Platform for Three Poles [dataset], 10.11888/Snow.tpd.271556, 2021.

448 Luoju, K., Pulliainen, J., Takala, M., Lemmetyinen, J., Mortimer, C., Derksen, C., Mudryk, L., Moisander, M., Hiltunen,  
449 M., and Smolander, T.: GlobSnow v3. 0 Northern Hemisphere snow water equivalent dataset, *Scientific Data*, 8, 1-16, 2021.

450 Mann, H. B.: Nonparametric test against trend, *Econometrica*, 13, 245-259, 1945.

451 Menne, M., Durre, I., Korzeniewski, B., McNeal, S., Thomas, K., Yin, X., Anthony, S., Ray, R., Vose, R., and Gleason, B.:  
452 Global Historical Climatology Network–Daily (GHCN-Daily), Version, 3, V5D21VHZ, 2016.

453 Mortimer, C., Mudryk, L., Derksen, C., Luoju, K., Brown, R., Kelly, R., and Tedesco, M.: Evaluation of long-term Northern  
454 Hemisphere snow water equivalent products, *The Cryosphere*, 14, 1579-1594, 2020.

455 Mudryk, L., Derksen, C., Kushner, P., and Brown, R.: Characterization of Northern Hemisphere snow water equivalent  
456 datasets, 1981–2010, *Journal of Climate*, 28, 8037-8051, 2015a.

457 Mudryk, L. R., Derksen, C., Kushner, P. J., and Brown, R.: Characterization of Northern Hemisphere Snow Water Equivalent  
458 Datasets, 1981-2010, *J Climate*, 28, 8037-8051, 10.1175/Jcli-D-15-0229.1, 2015b.

459 Muñoz Sabater, J.: ERA5-Land hourly data from 1981 to present, Copernicus Climate Change Service (C3S) Climate Data  
460 Store (CDS), 2019.

461 Ntokas, K. F., Odry, J., Boucher, M.-A., and Garnaud, C.: Investigating ANN architectures and training to estimate snow  
462 water equivalent from snow depth, *Hydrology and Earth System Sciences*, 25, 3017-3040, 2021.

463 Pan, M., Fisher, C. K., Chaney, N. W., Zhan, W., Crow, W. T., Aires, F., Entekhabi, D., and Wood, E. F.: Triple collocation:  
464 Beyond three estimates and separation of structural/non-structural errors, *Remote Sens Environ*, 171, 299-310,  
465 10.1016/j.rse.2015.10.028, 2015.

466 Pan, M., Sheffield, J., Wood, E. F., Mitchell, K. E., Houser, P. R., Schaake, J. C., Robock, A., Lohmann, D., Cosgrove, B.,  
467 and Duan, Q.: Snow process modeling in the North American Land Data Assimilation System (NLDAS): 2. Evaluation of  
468 model simulated snow water equivalent, *Journal of Geophysical Research: Atmospheres*, 108, 2003.

469 Pulliainen, J.: Mapping of snow water equivalent and snow depth in boreal and sub-arctic zones by assimilating space-borne  
470 microwave radiometer data and ground-based observations, *Remote Sens Environ*, 101, 257-269, 10.1016/j.rse.2006.01.002,  
471 2006.

472 Pulliainen, J., Luojus, K., Derksen, C., Mudryk, L., Lemmetyinen, J., Salminen, M., Ikonen, J., Takala, M., Cohen, J.,  
473 Smolander, T., and Norberg, J.: Patterns and trends of Northern Hemisphere snow mass from 1980 to 2018 (vol 41, pg 861,  
474 2020), *Nature*, 582, E18-E18, 10.1038/s41586-020-2416-4, 2020.

475 Reichle, R. H., Koster, R. D., De Lannoy, G. J. M., Forman, B. A., Liu, Q., Mahanama, S. P. P., and Toure, A.: Assessment  
476 and Enhancement of MERRA Land Surface Hydrology Estimates, *J Climate*, 24, 6322-6338, 10.1175/Jcli-D-10-05033.1,  
477 2011.

478 Rodell, M., Houser, P., Jambor, U., Gottschalck, J., Mitchell, K., Meng, C.-J., Arsenault, K., Cosgrove, B., Radakovich, J.,  
479 and Bosilovich, M.: The global land data assimilation system, *Bulletin of the American Meteorological Society*, 85, 381-394,  
480 2004.

481 Saleh, A. M. E., Arashi, M., and Kibria, B. G.: Theory of ridge regression estimation with applications, John Wiley &  
482 Sons 2019.

483 Santi, E., Brogioni, M., Leduc-Leballeur, M., Macelloni, G., Montomoli, F., Pampaloni, P., Lemmetyinen, J., Cohen, J., Rott,  
484 H., and Nagler, T.: Exploiting the ANN Potential in Estimating Snow Depth and Snow Water Equivalent From the Airborne  
485 SnowSAR Data at X-and Ku-Bands, *IEEE Transactions on Geoscience and Remote Sensing*, 2021.

486 Snauffer, A. M., Hsieh, W. W., and Cannon, A. J.: Comparison of gridded snow water equivalent products with in situ  
487 measurements in British Columbia, Canada, *J Hydrol*, 541, 714-726, 10.1016/j.jhydrol.2016.07.027, 2016.

488 Snauffer, A. M., Hsieh, W. W., Cannon, A. J., and Schnorbus, M. A.: Improving gridded snow water equivalent products in  
489 British Columbia, Canada: multi-source data fusion by neural network models, *Cryosphere*, 12, 891-905, 10.5194/tc-12-891-  
490 2018, 2018.

491 Stocker, T.: *Climate change 2013: the physical science basis: Working Group I contribution to the Fifth assessment report of*  
492 *the Intergovernmental Panel on Climate Change*, Cambridge university press 2014.

493 Tedesco, M. and Jeyaratnam, J.: AMSR-E/AMSR2 Unified L3 Global Daily 25 km EASE-Grid Snow Water Equivalent,  
494 Version 1.[online] Boulder, Colorado USA, NASA National Snow and Ice Data Center Distributed Active Archive Center,  
495 2019.

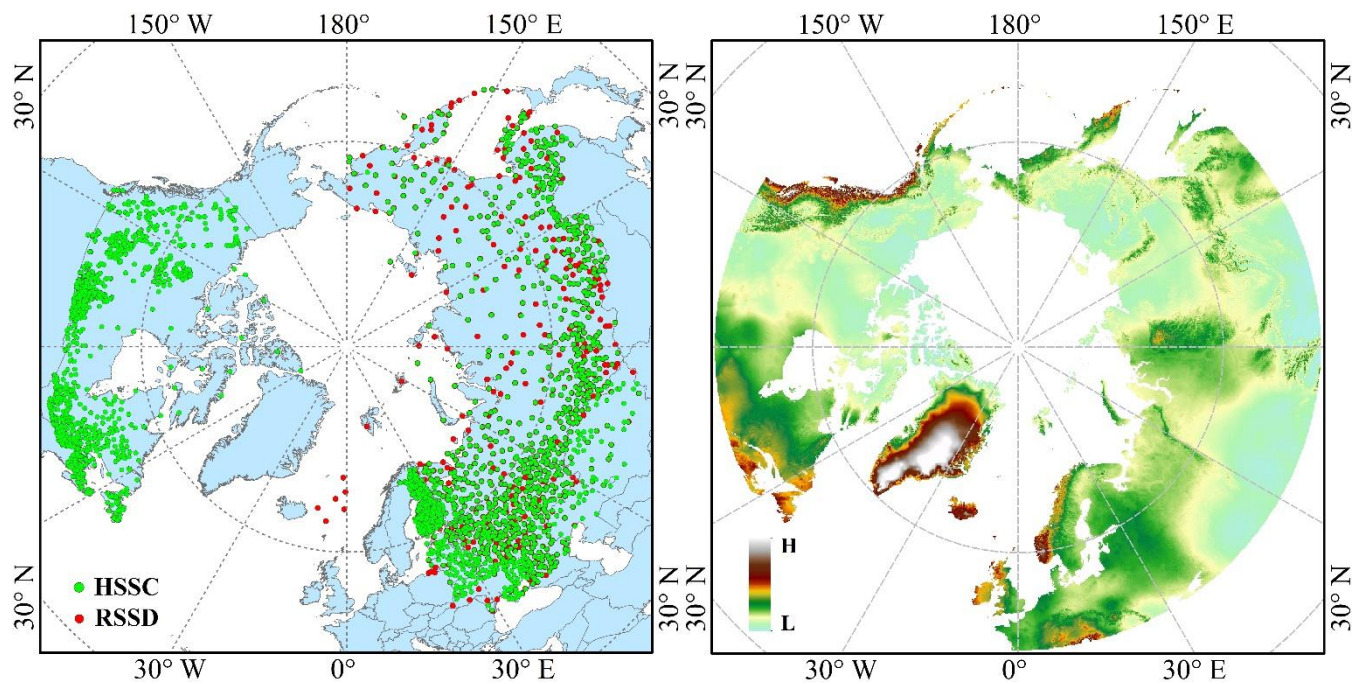
496 Vuyovich, C. M., Jacobs, J. M., and Daly, S. F.: Comparison of passive microwave and modeled estimates of total watershed  
497 SWE in the continental U nited S tates, *Water resources research*, 50, 9088-9102, 2014.

498 Walker, A., Brasnett, B., and Brown, R.: Canadian Meteorological Centre (CMC) daily gridded snow depth analysis for  
499 Northern Hemisphere, 1998-2008, 2011.

500 Wang, J. W., Yuan, Q. Q., Shen, H. F., Liu, T. T., Li, T. W., Yue, L. W., Shi, X. G., and Zhang, L. P.: Estimating snow depth  
501 by combining satellite data and ground-based observations over Alaska: A deep learning approach, *J Hydrol*, 585, ARTN  
502 124828  
503 10.1016/j.jhydrol.2020.124828, 2020.

504 Xiao, X. X., Zhang, T. J., Zhong, X. Y., Shao, W. W., and Li, X. D.: Support vector regression snow-depth retrieval algorithm  
505 using passive microwave remote sensing data, *Remote Sens Environ*, 210, 48-64, 10.1016/j.rse.2018.03.008, 2018.

506  
507



508

509

**Figure 1: The DEM and snow survey stations of the research region. The right subgraph shows the DEM and the left subgraph shows the SWE observational stations. HSSC, hemispheric-scale snow course; RSSD, the Russian snow survey station. The spatial range of the RRM SWE product is consistent with that of the DEM.**

512

513

**Table 1: Introduction to the SWE data.**

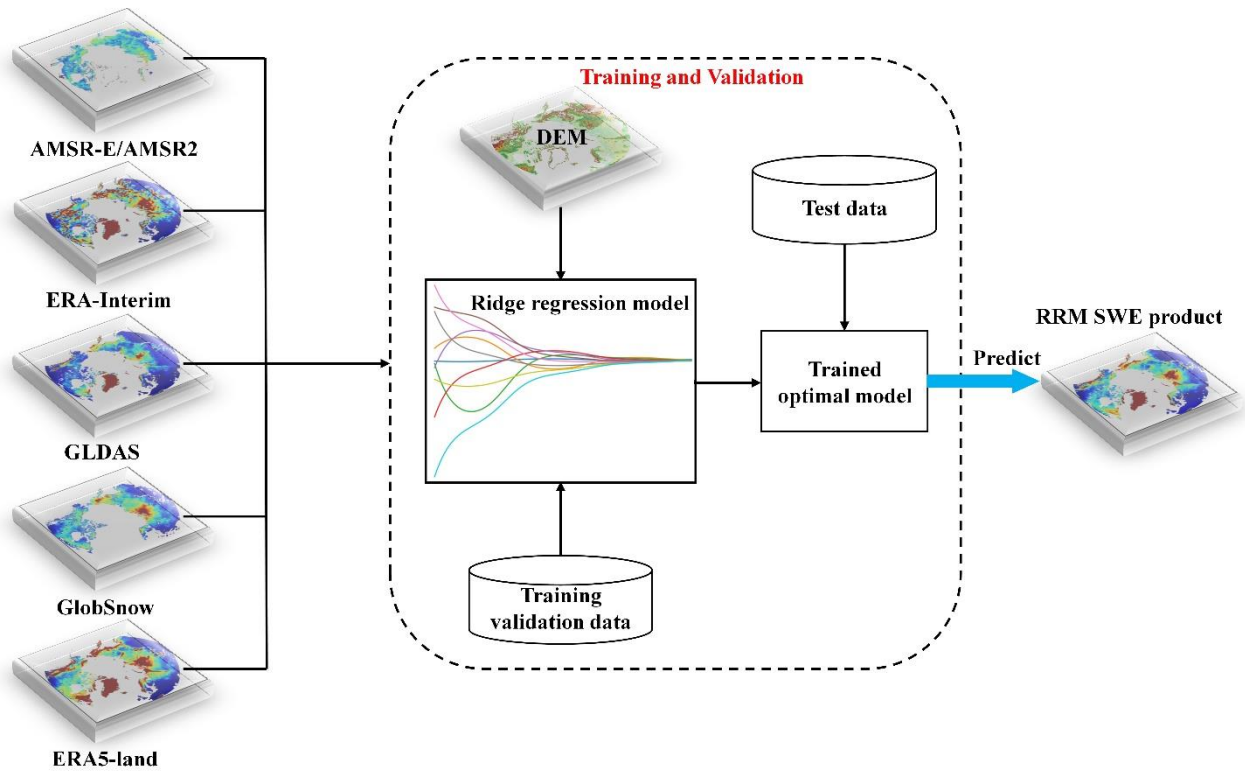
<b>Data type</b>	<b>Data name</b>	<b>Time series</b>	<b>Temporal resolution</b>	<b>Spatial resolution</b>	<b>Spatial coverage</b>	<b>File format</b>
Remote sensing data	AMSR-E/AMSR2	2002-2011/2012-2020	Daily	25 km x 25 km	Global (No Greenland)	HDF5
Data assimilation dataset	GLDAS	1979-2020	Daily	0.25°×0.25°	Global	NetCDF
	GlobSnow	1979-2018	Daily	0.25°×0.25°	Northern Hemisphere (No Greenland)	NetCDF
Reanalysis dataset	ERA-Interim	1979-2019	Daily	0.25°×0.25°	Global	NetCDF
	ERA5-land	1981- present	Hour	0.1°×0.1°	Global	NetCDF

515

516

517





518

519

Figure 2: Flow chart of the RRM SWE data preparation (preparation of spatiotemporal seamless SWE datasets mainly includes

520

three processes: model training, model reasoning, and SWE data preparation).

521

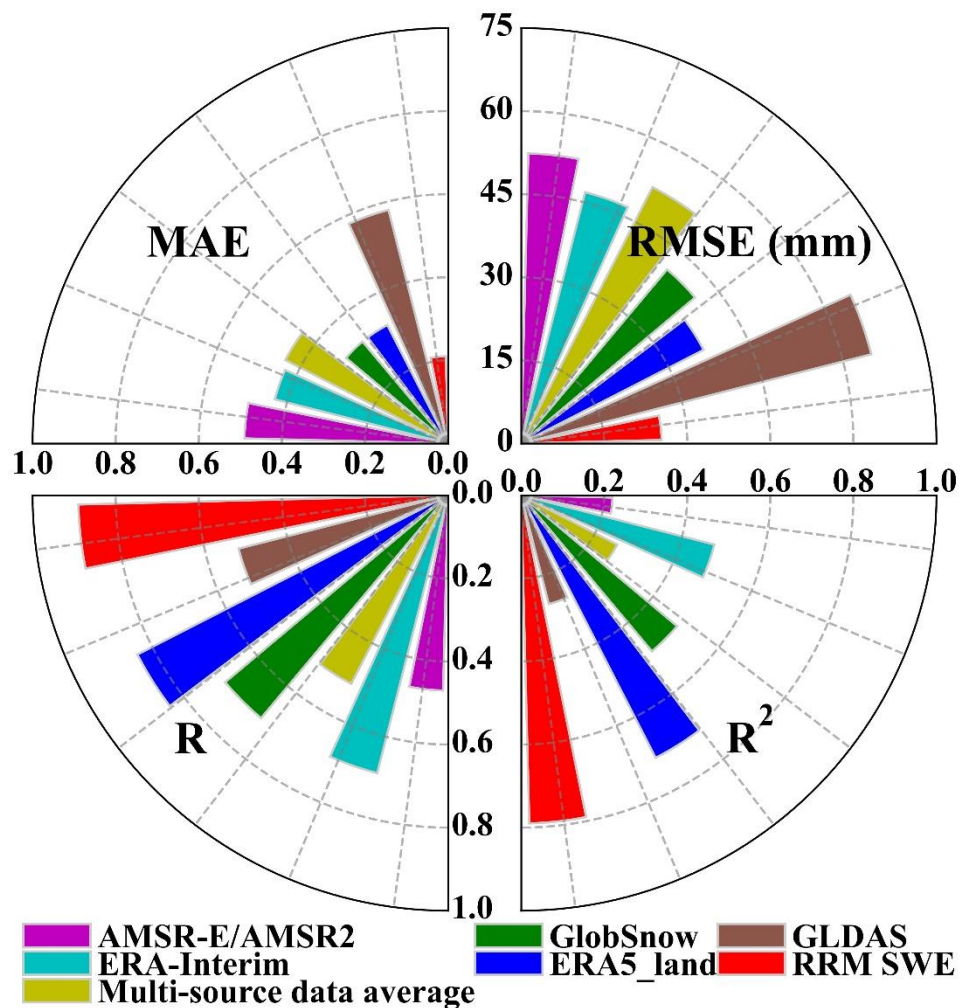
522

523 **Table 2: Error list for the station data and grid snow water equivalent products.**

<b>Error type</b>	<b>MAE</b>	<b>RMSE (mm)</b>	<b>R</b>	<b>R<sup>2</sup></b>
ERA-Interim	0.43	46.81	0.69	0.48
AMSR-E/AMSR2	0.49	52.39	0.47	0.22
GLDAS	0.58	65.25	0.52	0.27
GlobSnow	0.32	40.99	0.70	0.49
ERA5-land	0.32	37.02	0.84	0.71
Multisource data average	0.44	52.00	0.51	0.26
RRM SWE	0.21	25.37	0.89	0.79

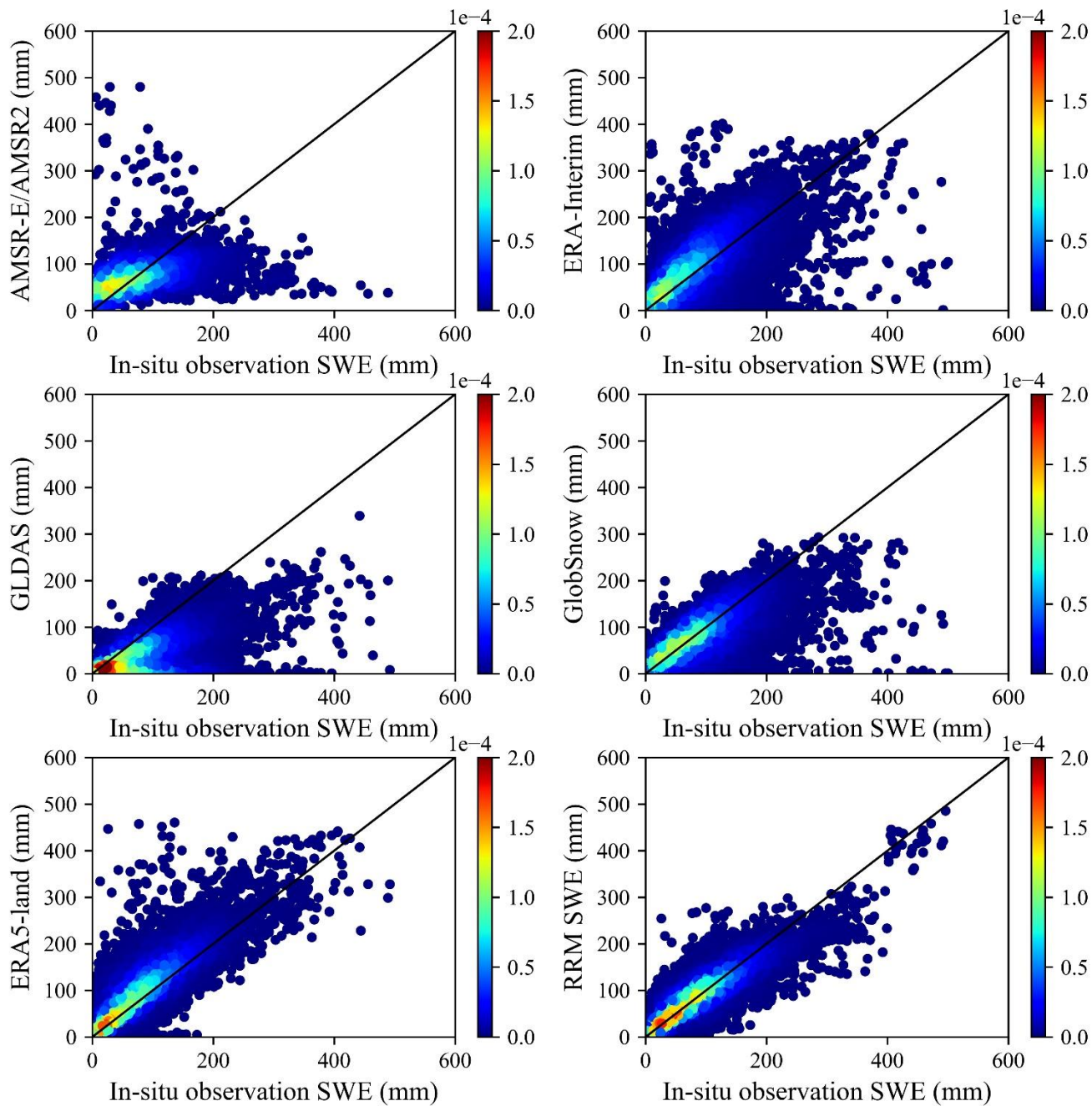
524

525



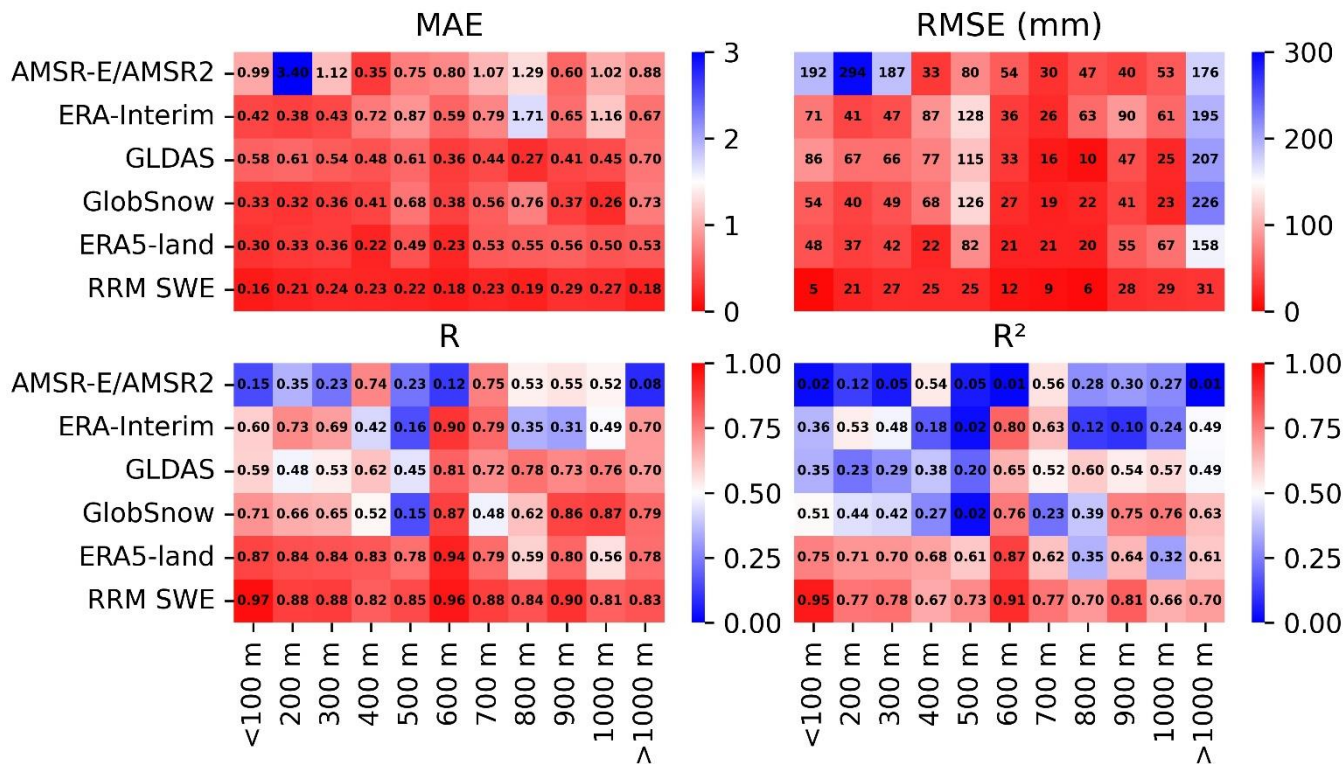
526

527 **Figure 3:** Accuracy comparison of various SWE products. The upper left sector represents the MAE, the upper right sector  
 528 represents the RMSE, the lower-left sector represents R, and the lower right sector represents R<sup>2</sup>. The sector axis represents the  
 529 size of the error, and the color represents different SWE datasets.



530

531 **Figure 4: Error verification density diagram (a total of 38807 sample points were used for verification). The color bar represents**  
 532 **the value of kernel density estimation. The closer the high-density area is to the 1:1 line, the higher the verification accuracy of the**  
 533 **dataset is at most of the measuring stations.**



534

535

536

537

538

539

540

541

542

543

544

545

546

547

548

549

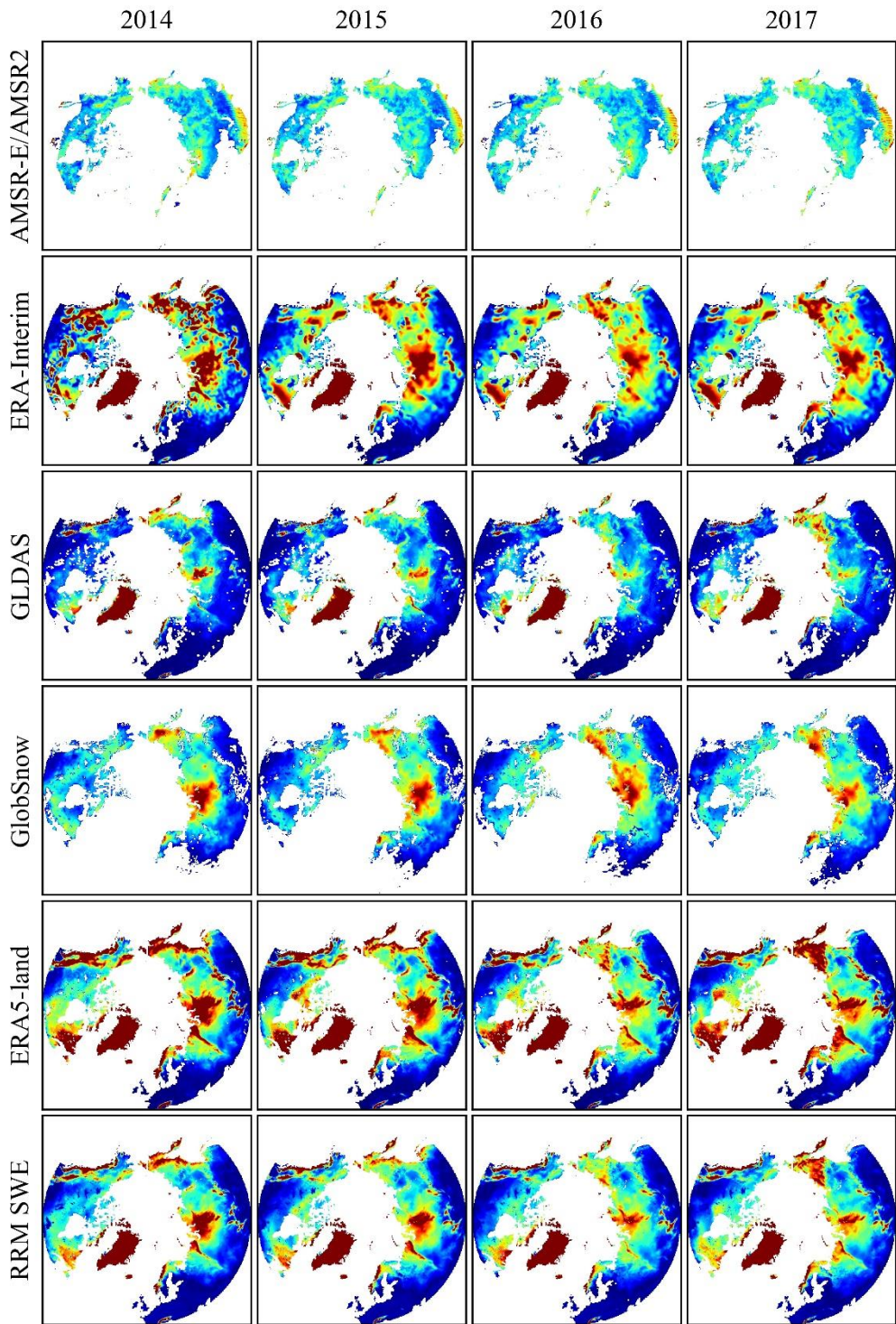
550

Figure 5: Comparison of the error between the RRM SWE and AMSR-E/AMSR2 SWE, ERA-Interim SWE, GLDAS SWE, GlobSnow SWE, and ERA5-land SWE at different altitudes (the abscissa represents the altitude gradient, and the ordinate represents different SWE datasets). The color bar indicates the error in each SWE dataset. The closer to red the color is, the higher the accuracy is. MAE: mean absolute error, RMSE: root mean square error, R: Pearson's correlation coefficient, R<sup>2</sup>: coefficient of determination).

551 **Table 3: Error list for the station data and RRM SWE product in different regions.**

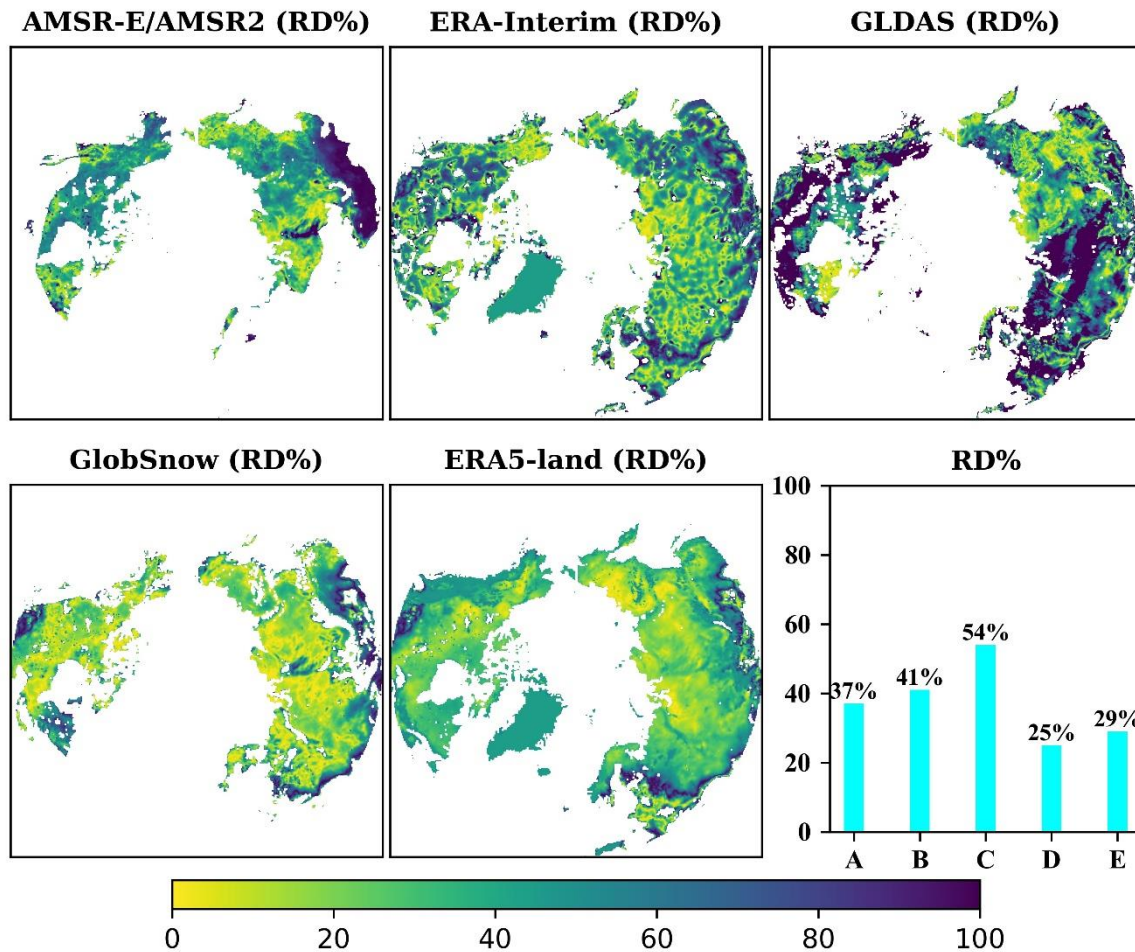
<b>Region</b>	<b>MAE</b>	<b>RMSE (mm)</b>	<b>R</b>	<b>R<sup>2</sup></b>
Russia	0.20	26.39	0.89	0.79
Canada	0.23	29.31	0.87	0.76
Finland	0.21	25.29	0.89	0.79

552



554 **Figure 6: Comparison of the spatial distribution characteristics between the RRM SWE and AMSR-E/AMSR2 SWE, ERA-**  
555 **Interim SWE, GLDAS SWE, GlobSnow SWE, and ERA5-land SWE (the four columns of images represent the comparison results**  
556 **in 2014, 2015, 2016, and 2017, respectively).**  
557





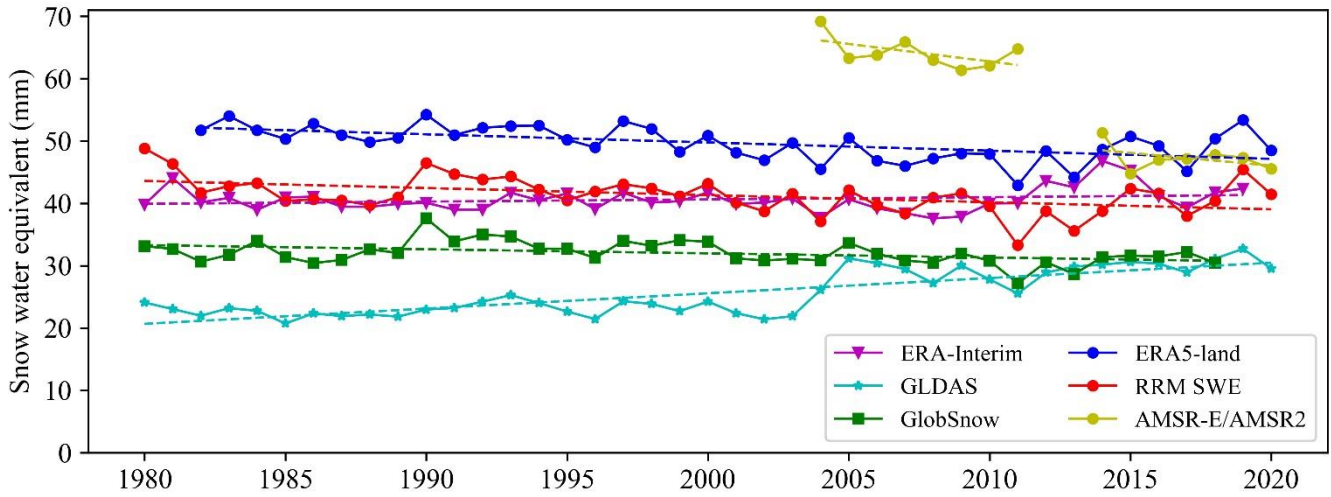
558

559 **Figure 7: Temporal and spatial distributions of relative differences (RD%) between the RRM SWE and AMSR-E/AMSR2 SWE,**

560 **ERA-Interim SWE, GLDAS SWE, GlobSnow SWE, and ERA5-land SWE. Lower-right subgraph: Comparison of annual average**

561 **relative differences between the RRM SWE and AMSR2 SWE (A), ERA-Interim SWE (B), GLDAS SWE (C), GlobSnow SWE**

562 **(D), and ERA5-land SWE (E).**



563

564

**Figure 8: Annual variation tendency in the AMSR-E/AMSR2 SWE, ERA-Interim SWE, GLDAS SWE, GlobSnow SWE, ERA5-land SWE and RRM SWE products from 1979 to 2019 (the dotted line is the trend line calculated based on the Mann-Kendall method).**

565

566

567

**Table 4: Results of the Mann-Kendall trend test performed for various snow water equivalent products for 1979 to 2019.**

<b>Data</b>	<b>P-value</b>	<b>Test value</b>	<b>Trend</b>
AMSR-E/AMSR2	0.00	-3.26	Decreasing
ERA-Interim	0.27	1.08	No trend
GLDAS	7.29e-07	4.95	Increasing
GlobSnow	0.01	-2.54	Decreasing
ERA5-land	0.00	-3.43	Decreasing
RRM SWE	0.00	-3.00	Decreasing

\*Significance level  $\alpha = 0.05$